**SUPPLEMENTAL TABLE 1. Summary of Work in Ultrasound and Laser-Based Vaporization of Perfluorocarbon Nanodroplets**

| Ultrasound Based Vaporization | | | | | | | | | | |
|---|---|---|---|---|---|---|---|---|---|---|
| **Ref #** | Perfluorocarbon | Shell | Size (nm) | Frequency (MHz) | $P_{neg}$ (Mpa) | M.I. | Cycles | Environment | Temp (°C) | Notes |
| 1 | Perfluoropentane | PEG-PLLA | 590 | 1 | 0.74-1.24 | 0.7-1.2 | N/A | 0.6% Agrose Gel | 37 | |
| 2 | Perfluoropentane Perfluorohexane | DPPC, DPPA, PEG-DPPE (8:1:1) | 370-385 | 3.3 | 9 | 4.9 | 100 | Water, 3, 5, 10, 15, 20% Polyacrylamide Gels | 37 | |
| 3 | Perfluoropentane Perfluorohexane | DPPC, DPPA, PEG-DPPE (8:1:1) | 390 | 1.1 | 2.4 | 2.3 | 100 | 10% Polyacrylamide Gel | 37 | |
| 4 | Perfluoropentane | Albumin | 260 | 2 | 6 | 4.2 | 5 | 8% Polyacrylamide Gel | 37 | |
| 5 | Perfluoropentane | PEG-PLLA | 590 | 1 | 0.2-0.23 | 0.2-0.3 | N/A | 0.6% Agrose Gel | 37 | |
| 6 | perfluoro-15-crown-5-ether | PEG-PLLA | 275 | 1 | 0.34.0.41 | 0.3-0.4 | N/A | 0.6% Agrose Gel | 37 | |
| 7 | Perfluoropentane | Zonyl FSP | 400 | 7.5 | 1.5-2.2 | 0.6 - 0.8 | 5 - 50 | Water | 37 | |
| 8 | Perfluorobutane | DPPC, DPPE-PEG-200,TAP (65:5:30) | 200-300 | 5 | 2.7 or 3.8 | 1.2 or 1.7 | 10 | Water | 37 | Condensation based synthesis |
| 9 | Perfluoropentane | DPPC, DSPE-PEG2000 | 100, 200 | 3.3 | 3.8 | 2.1 | 30 | 8% Polyacrylamide Gel | 37 | |
| 10 | Perfluorhexane | Zonyl FSP | 260 | 1, 18 | 2.1, 6.3 | 2.1 to 1.4 | N/A | Intracellular Droplets | 37 | Vaporized after 2 hr growth |
| 11 | Perfluoropentane | DSPC, DSPE-PEG5000 | >300 | 3.2 | <4.3 | <1.5 | 100 | Water | 37 | Microfluidic based synthesis, only droplets >900 nm vaporized |
| 12 | Perfluorobutane, Perfluoropropane | DPPC, LPC, DPPE-PEG2000 | 200-300 | 5 | 2.7, 3.8 | 1.2 to 1.7 | 10 | Water | 22 | Condensation based synthesis |
| 13 | Octafluropropane | DSPC. DSPE-PEG2000 | 300 | 7.5 | 0.5, 2.0, 3.5 | to 1.3 | 2 | PBS | 22,37 | Condensation based synthesis |
| 14 | Perfluoropentane | Zonyl FSP | 200 | 10 | 6 | 1.9 | N/A | KHT-C tumor xenograph | 37 | *In vivo* results |
| **Non-Ultrasound Base Vaporization** | | | | **Details** | | | | | | |
| 15 | Perfluoropentane | Albumin | 200 - 400 | Loaded with gold nanorods. 2 - 10 mJ/cm$^2$ required, *in vitro* phantom and *in* vivo | | | | | | |
| 16 | Perflurohexane | Zonyl FSP | > 1000 | Loaded with silica-coated gold nanospheres, 50-120 mJ/cm$^2$ required, *in vitro* water and phantoms environment | | | | | | Micrometer scale droplets vaporized |

$P_{neg}$ is the peak negative pressure emitted by the excitation transducer. M.I. is the mechanical index, or the likelihood to produce bioeffects due to ultrasonic energy deposition. The FDA limits ultrasound exposure to an M.I. of 1.9. Most diagnostic ultrasound is operating at an M.I. approximately 10 times less than the FDA limit. Color indicates relative safety levels: green is considered safe, yellow is most likely safe, red could cause unwanted bioeffects. Environment indicates the medium in which the droplets were located during vaporization (*1*–*16*).

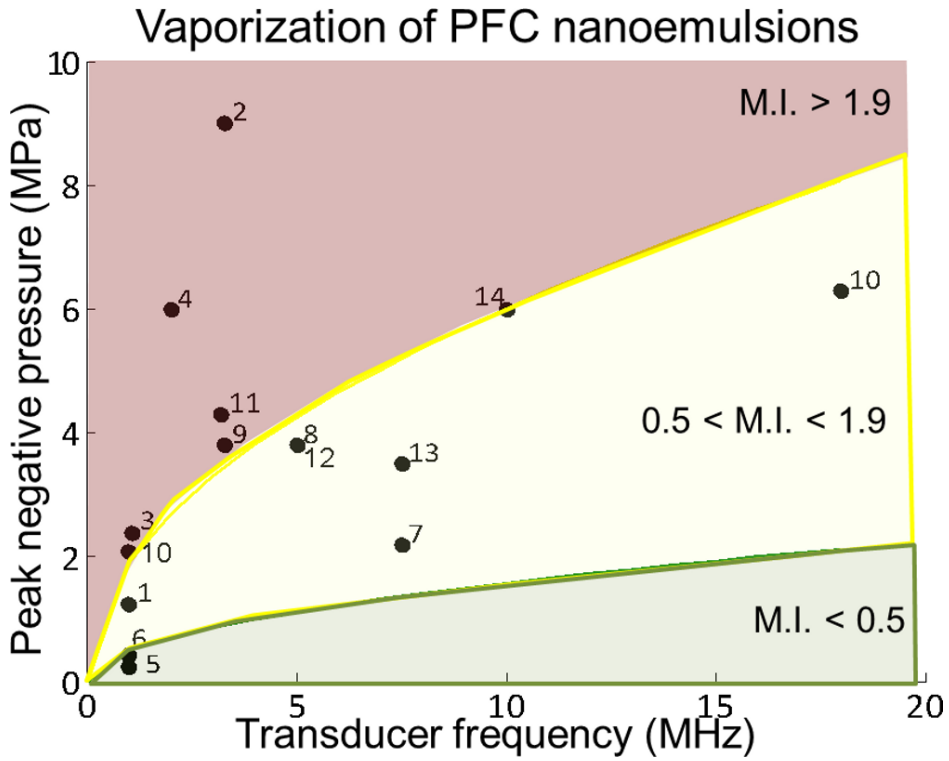


**SUPPLEMENTAL FIGURE 1.** Collection of acoustic parameters (transducer frequency, peak negative pressure, and corresponding M.I.) applied in several studies using ultrasound to vaporize nanodroplet emulsions (<500 nm). Numbers correspond to references listed in Supplemental Table 1 with further details.

## Endogenous Photoacoustic Contrast

Endogenous contrast-based molecular photoacoustic imaging of cancer has primarily focused on the oxygenation states of blood (*17*) (oxygenated and deoxygenated hemoglobin have substantially different absorption properties); however, other tissue chromophores including melanin, lipids, and water are also being explored (*18*). Spectroscopic photoacoustic imaging uses a priori knowledge of the absorption properties of tissue constituents and correlates the changes in photoacoustic amplitude taken over multiple wavelengths with the different absorbers via statistical methods (*19*). Imaging of blood and the oxygenation status of blood are two of the primary imaging principles for native photoacoustics and could be applied in cancer imaging (Fig. 3)[ID]FIG3[/ID]. Varying vascularization and oxygenation status is characteristic of many solid tumors (*20*) and can be quantified by photoacoustic imaging. Increased vascularization, such as in cancer, may produce an increase in photoacoustic signal allowing tumors to appear different from normal tissues in native photoacoustic images (*19*). However, the signal-to-noise ratio can be limited when intrinsic photoacoustic imaging is applied, because of the relatively high background imaging signal (normal tissue is also well vascularized and oxygenated). To further improve endogenous photoacoustic imaging, current research centers around the selection of appropriate imaging wavelengths and more accurate spectroscopic correlation methods and modeling (*19,21*). Alternatively, the introduction of exogenous photoacoustic contrast agents can substantially increase the contrast-to-noise ratio of photoacoustic molecular imaging.

## Exogenous Photoacoustic Contrast

Exogenous photoacoustic contrast agents consist of a range of small molecule and nanoparticles that absorb light and produce signal significantly higher than tissue photoabsorbers. Carbon nanotubes, iron oxide particles, and organic dyes have all served as photoacoustic contrast agents (*22*). The most frequently used contrast agents, however, are plasmonic noble metal nanoparticles because of superior optical absorption properties from their ability to undergo surface plasmon resonance (collective oscillations of free surface electrons due to laser irradiation). Because the size and shape of the particle determines the number and orientation of free surface electrons that can interact with

different wavelengths of light, the absorption peaks can therefore be altered via changing chemical synthesis parameters to provide absorption at the desired wavelength. Typically made from gold and silver, these particles are usually less than 80 nm in their largest dimension and have been synthesized in many shapes including nanospheres, nanoshells, nanorods, nanocages, and silica-coated gold and silver particles (Fig. 2) to enhance stability and increase signal (*22*). Dual-contrast agents for combined ultrasound and photoacoustic imaging have also been developed to leverage the complementary character of both techniques. Vaporizing liquid perfluorocarbon droplets (for acoustic contrast) in which optically absorbing nanoparticles are embedded (gold nanorods (*23* or lead sulfide nanospheres (*24*)) provide dual-contrast images through 3 mechanisms: light irradiates these particles, the localized thermal expansion creates a high-frequency pressure wave, and the wave vaporizes the surrounding liquid perfluorocarbon. This vaporization event produces a strong photoacoustic imaging signal substantially higher than signal from thermoelastic expansion. In addition to the 2 photoacoustic imaging signals, the phase change of perfluorocarbon into gas provides ultrasonic contrast through an increased change in acoustic impedance at the site of particle vaporization, compared with surrounding tissue, allowing for directly coregistered, molecularly specific ultrasound and photoacoustic contrast (Fig. 2). Some recent reviews provide more details on different photoacoustic contrast agents (*19,21,22*).

## Supplemental References


1. Rapoport NY, Efros AL, Christensen DA, Kennedy AM, Nam KH. Microbubble generation in phase-shift nanoemulsions used as anticancer drug carriers. *Bubble Sci Eng Technol*. 2009;1:31–39.
2. Asami R, Ikeda T, Azuma T, Umemura S, Kawabata K. Acoustic signal characterization of phase change nanodroplets in tissue-mimicking phantom gels. *Jpn J Appl Phys*. 2010;49:07HF16/1–07HF16/6.
3. Kawabata K, Asami R, Azuma T, Umemura S. Acoustic response of microbubbles derived from phase-change nanodroplet. *Jpn J Appl Phys*. 2010;49:07HF18/1–07HF18/9.
4. Zhang P, Porter T. An in vitro study of a phase-shift nanoemulsion: a potential nucleation agent for bubble-enhanced HIFU tumor ablation. *Ultrasound Med Biol*. 2010;36:1856–66.
5. Rapoport N, Nam K-H, Gupta R, et al. Ultrasound-mediated tumor imaging and nanotherapy using drug loaded, block copolymer stabilized perfluorocarbon nanoemulsions. *J Control Release*. 2011;153:4–15.
6. Rapoport N, Gao Z, Kennedy A. Multifunctional nanoparticles for combining ultrasonic tumor imaging and targeted chemotherapy. *J Natl Cancer Inst*. 2007;99:1095–1106.
7. Reznik N, Williams R, Burns PN. Investigation of vaporized submicron perfluorocarbon droplets as an ultrasound contrast agent. *Ultrasound Med Biol*. 2011;37:1271–9.
8. Sheeran PS, Luois S, Dayton PA, Matsunaga TO. Formulation and acoustic studies of a new phase-shift agent for diagnostic and therapeutic ultrasound. *Langmuir*. 2011;27:10412–10420.
9. Kopechek JA, Zhang P, Burgess MT, Porter TM. Synthesis of phase-shift nanoemulsions with narrow size distributions for acoustic droplet vaporization and bubble-enhanced ultrasound-mediated ablation. *J Vis Exp*. 2012:e4308.
10. Martin AL, Seo M, Williams R, Belayneh G, Foster FS, Matsuura N. Intracellular growth of nanoscale perfluorocarbon droplets for enhanced ultrasound-induced phase-change conversion. *Ultrasound Med Biol*. 2012;38:1799–810.
11. Martz TD, Bardin D, Sheeran PS, Lee AP, Dayton PA. Microfluidic generation of acoustically active nanodroplets. *Small*. 2012;8:1876–1879.
12. Matsunaga TO, Sheeran PS, Luois S, et al. Phase-change nanoparticles using highly volatile perfluorocarbons: toward a platform for extravascular ultrasound imaging. *Theranostics*. 2012;2:1185–98.
13. Sheeran PS, Luois SH, Mullin LB, Matsunaga TO, Dayton PA. Design of ultrasonically-activatable nanoparticles using low boiling point perfluorocarbons. *Biomaterials*. 2012;33:3262–3269.

14. Williams R, Wright C, Cherin E, et al. Characterization of submicron phase-change perfluorocarbon droplets for extravascular ultrasound imaging of cancer. *Ultrasound Med Biol*. 2013;39:475–489.

15. Wilson K, Homan K, Emelianov S. Biomedical photoacoustics beyond thermal expansion using triggered nanodroplet vaporization for contrast-enhanced imaging. *Nat Commun*. 2012;3:618.

16. Strohm EM, Gorelikov I, Matsuura N, Kolios MC. Acoustic and photoacoustic characterization of micron-sized perfluorocarbon emulsions. *J Biomed Opt*. 2012;17:96011–96016.

17. Herzog E, Taruttis A, Beziere N, Lutich AA, Razansky D, Ntziachristos V. Optical imaging of cancer heterogeneity with multispectral optoacoustic tomography. *Radiology*. 2012;263:461–468.

18. Mallidi S, Luke GP, Emelianov S. Photoacoustic imaging in cancer detection, diagnosis, and treatment guidance. *Trends Biotechnol*. 2011;29:213–221.

19. Luke GP, Yeager D, Emelianov SY. Biomedical applications of photoacoustic imaging with exogenous contrast agents. *Ann Biomed Eng*. 2012;40:422–437.

20. Prabhakar U, Maeda H, Jain RK, et al. Challenges and key considerations of the enhanced permeability and retention effect (EPR) for nanomedicine drug delivery in oncology. *Cancer Res*. 2013;73:2412–2417.

21. Beard P. Biomedical photoacoustic imaging. *Interface Focus*. 2011;1:602–631.

22. Su JL, Wang B, Wilson KE, et al. Advances in clinical and biomedical applications of photoacoustic imaging. *Expert Opin Med Diagn*. 2010;4:497–510.

23. Wilson K, Homan K, Emelianov S. Biomedical photoacoustics beyond thermal expansion using triggered nanodroplet vaporization for contrast-enhanced imaging. *Nat Commun*. 2012;3:618.

24. Rapoport N. Phase-shift, stimuli-responsive perfluorocarbon nanodroplets for drug delivery to cancer. *Wiley Interdiscip Rev Nanomed Nanobiotechnol*. 2012;4:492–510.